Applied Catalysis B: Environmental 249 (2019) 1–8

Contents lists available at ScienceDirect

Applied Catalysis B: Environmental

journal homepage: www.elsevier.com/locate/apcatb

One-step construction of Pickering emulsion via commercial TiO_2 nanoparticles for photocatalytic dye degradation

Qin Li*, Tingting Zhao, Mei Li*, Wenting Li, Bin Yang, Dongran Qin, Kangle Lv, Xian Wang, Lamei Wu, Xiaofeng Wu, Jie Sun

Key Laboratory of Resources Green Conversion and Utilization of the State Ethnic Affairs Commission & Ministry of Education, South-Central University for Nationalities, Wuhan 430074, PR China

ARTICLE INFO

Keywords:
Pickering emulsion
TiO_2
Hydrophilicity
Dye
Photocatalysis

ABSTRACT

Pickering emulsion (PE) stabilized by semiconductors for photocatalysis applications has received growing endorsement over the last decade due to its high interfacial activity. However, since most semiconductors inherently possess a strongly hydrophilic or hydrophobic surface and are unable to stabilize PE microcapsules by themselves, pretreating the surface of semiconductor powder with foreign modifier was usually unavoidable and inconvenient before the PE construction. Even worse, the added modifier inevitably limited the contact between the semiconductor and the reactant during the photocatalysis process. Herein, an oil-in-water PE was successfully obtained in one step without pretratment of the semiconductor, where the dye-contained wastewater and insoluble organic matter acted as the water and oil phases, respectively, and the dye molecules in water could directly assist TiO_2 particles to become the stabilizer. The TiO_2 powder in the formed PE system exhibited markedly enhanced photoactivity for dye degradation over that in traditional non-emulsified systems, and the PE microcapsules could be easily recovered for reuse and withstand long-term irradiation without severe demulsification. This work not only highlights a convenient and promising approach to build Pickering emulsion as a novel photocatalytic system with extremely high efficiency and recyclability, but also provides a new way of thinking on how to simplify the PE construction to meet more requirement in future practical applications.

1. Introduction

In 1907, Spencer Pickering discovered that amphiphilic solid particles could be spontaneously immobilized at the water-oil interface to form a thermodynamically stable emulsion, henceforth called a Pickering emulsion (PE) [1]. To reduce the interfacial tension between water, oil and solid, the solid particles tend to uniformly and closely arrange in a few layers at the water-oil interface [2–8]. In recent years, the concept of PE has increasingly attracted attention in the photocatalysis fields [9–11]. Photocatalysts in the form of PEs could offer the largest active surface area for photoreactions with pollutants in both the aqueous and oil phases. More significantly, the PE system strictly defines the distribution area of the photocatalyst (at the water-oil interface) in the absence of any additional substrate. Therefore, many of the problems associated with traditional photocatalytic systems, including agglomeration of the powder, a small reactive area, a low photocatalytic efficiency, and difficult recovery, are effectively overcome [12–15]. For example, Nsib et al. prepared an oil-in-water (o/w) PE using TiO_2 particles modified with salicylic acid as a stabilizer and monochlorobenzene (MCB) as both the oil phase and model contaminant [16], which offered an enhanced photodegradation activity over the nonemulsified system. Similar phenomena were also discovered for PE-based photocatalysis systems based on the $K_4Nb_6O_{17}$ intercalated with alkylammonium cations for the porphyrin decomposition [17], ZnO particles modified with a titanate coupling agent for the nitrobenzene degradation [18], and graphdiyne, graphene or carbon nanotubes functionalized Ag_3PO_4 for both the methylene blue degradation and the O_2 production from water splitting [19,20].

However, since most semiconductors inherently possess a strongly hydrophilic or hydrophobic surface and are unable to stabilize PE microcapsules by themselves [21], in those previous works, introducing foreign modifier to pretreat the particle surface usually made the synthetic process cumbersome, and the modifier inevitably limited the contact between the semiconductor particles and the target pollutant to a certain extent.

Herein, innovatively, a one-step strategy for the preparation of o/w PE was developed and applied in the photocatalytic dye degradation (see Scheme 1). A specific aqueous dye solution and an insoluble

* Corresponding authors.
E-mail addresses: liqin0518@mail.scuec.edu.cn (Q. Li), limei@mail.scuec.edu.cn (M. Li).

https://doi.org/10.1016/j.apcatb.2019.02.057
Received 27 October 2018; Received in revised form 18 January 2019; Accepted 20 February 2019
Available online 22 February 2019
0926-3373/

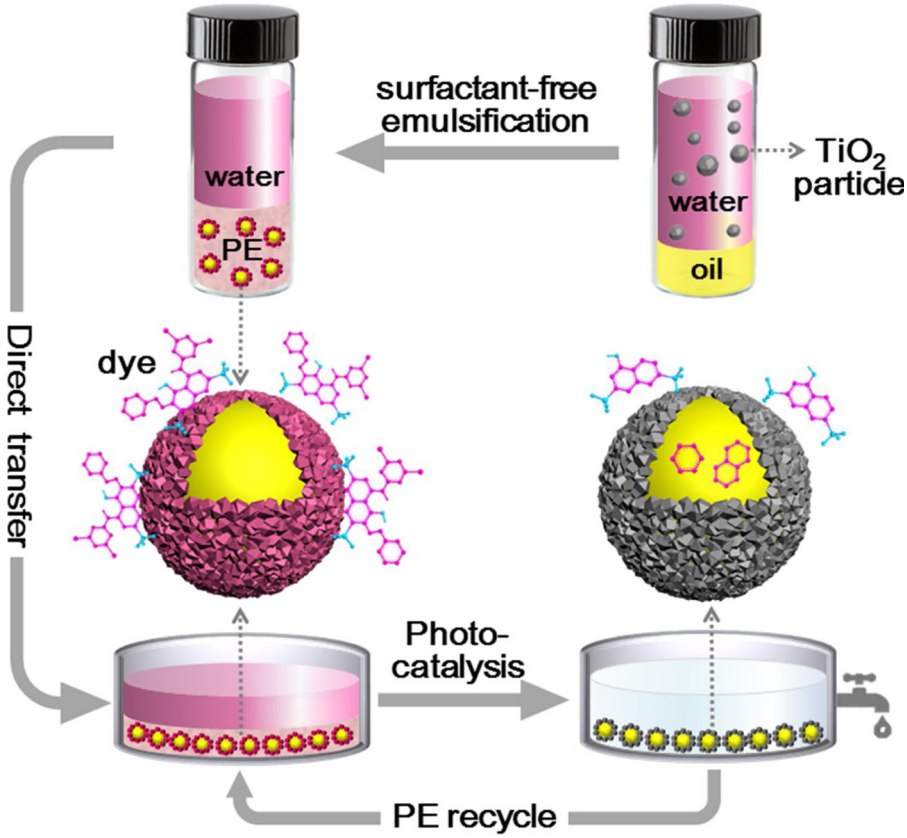

Scheme 1. Diagram of an o/w Pickering emulsion (PE) construction from superhydrophilic TiO_2 for photocatalytic dye degradation.

organic solvent dichloromethane (DCM) were employed as the continuous water phase and dispersive oil phase, respectively, and commercial anatase TiO_2 was used as the stabilizer. In this study, four dyes, reactive brilliant red X_3B, methyl orange (MO), Congo red (CR), and orange G (OG), were chosen as the research objects. The selection criteria would be discussed later. The solubilities of the four studied dyes in DCM were negligible (see Fig. S1). Therefore, compared with the case in the traditional systems, the addition of the oil in the Pickering emulsion system had a negligible effect on the initial concentration of dyes in the photocatalytic degradation process. Unlike in the case of surface-pretreated photocatalyst emulsions, the dye molecules directly contacted with TiO_2 in our designed system, which could effectively avoid screening of the interaction between the photocatalyst and contaminant by the extrinsic modifiers. To the best of our knowledge, this is the first example that stabilizes Pickering emulsion directly via commercial semiconductors for photocatalytic applications.

2. Experimental section

2.1. Materials

Anatase TiO_2 powder was purchased from Sigma-Aldrich. The dyes X_3B, MO, CR, OG, and fluorescein isothiocyanate (FITC) were bought from Aladdin Industrial Corporation. DCM and calcein were obtained from Sinopharm Chemical Reagent Co., Ltd. in China. Nile red was purchased from Shanghai Yuanye Biological Technology Co., Ltd. in China. Deionized (DI) water was used in all experiments.

2.2. Construction of Pickering emulsions

In a typical process, 50 mg of commercial anatase TiO_2 nanoparticles without any pretreatment was first dispersed in 20 mL of an aqueous X_3B solution (80 ppm) in a vial and vibrated overnight. After the addition of 3 mL of DCM into the dispersion, an o/w Pickering emulsion was successfully obtained by simply shaking the mixture by hand for approximately 2 min. Neither excess TiO_2 powder nor continuous oil should be present in the system; if either is present, the vial should be further shaken to complete the emulsification. In addition to X_3B, we also prepared MO-, CR-, and OG-based emulsion systems. The optimized preparation parameters are listed in Table 1.

2.3. Characterizations

Optical and fluorescence microscopy images of the formed Pickering microcapsules were obtained with an optical microscope (Olympus CX31) and a confocal laser scanning microscope (Leica TCS SP8), respectively. For fluorescence imaging, Nile red and calcein fluorescent dyes with a concentration of 100 μmol L^{-1} were used to color the oil and water phases, respectively, and FITC was used to tag the TiO_2 nanoparticles using the method reported in previous literature studies [22,23]. Briefly, 69 mg of 3-aminopropyltriethoxysilane (APTS) and 6 mg of FITC were combined in 10 mL of ethanol under an N_2 atmosphere and magnetically stirred for 12 h. The obtained fluorescent FITC–APTS conjugate solution was protected from light during reaction

Table 1
Preparation parameters of the PEs based on different dyes.

Dyes	Concentration (ppm)	S:O:W[a]	M_{solid} (mg)	V_{oil} (mL)	V_{water} (mL)
X_3B	80	50:3:20	50	3	20
MO	12	7:1:7	28	4	28
CR	100	6:3:10	18	9	30
OG	50	5:1:5	30	6	30

[a] S, O, W respectively refer to the solid phase (TiO_2), oil phase (DCM), and water phase (aqueous dye solution).

and storage to prevent photobleaching. Then, 1 mL of ammonium hydroxide ($NH_3{\cdot}H_2O$, 25 wt%) was combined with 30 mL of ethanol in a 100 mL round-bottom flask under magnetic stirring. After 5 min, 1.4 mL of $NH_3{\cdot}H_2O$ and 3 mg of TiO_2 powder were added, and the mixture was stirred for another 10 min. Then 0.5 mL of the FITC–APTS conjugate was added, and the mixture was magnetically stirred for 24 h in the dark. The precipitate was obtained by centrifugation and subsequently washed with DI water and ethanol several times until no fluorescence signal was detected in the supernatant. Then, the FITC-doped TiO_2 nanoparticles were dried with air. Afterward, 3 mg of the FITC-doped TiO_2 nanoparticles, 7 mg of TiO_2 powder, and 4 mL of an aqueous X_3B solution (80 ppm) were uniformly mixed in a vial and vibrated overnight. Lastly, 0.6 mL of DCM was added to the vial, and the mixture was emulsified for observation under the confocal laser scanning microscope.

The water contact angle was measured using digital image processing on a JC2000D1 optical contact angle meter (Shanghai Zhongchen Technology Co., China) by dripping 2 μL of DI water on the surface of a compressed sample tablet. Fourier transform infrared (FTIR) spectra of the samples were recorded between 400 and 2000 cm^{-1} on a Nicolet6700 FTIR spectrometer. The zeta potential and conductivity of the samples in 2.5 mL of aqueous slurry (0.5 mg mL^{-1}) were measured on a Malvern Zetasizer Nano ZS90 instrument at neutral pH. UV/vis diffuse reflectance absorption spectra (DRS) were obtained on a UV-2600 UV/vis spectrophotometry (Shimadzu, Japan) using $BaSO_4$ as the reflectance standard. The Brunauer-Emmett-Teller (BET) specific surface areas (S_{BET}) of the samples were analyzed by a nitrogen adsorption apparatus (Micromeritics ASAP 2020, USA). The sample powder was degassed at 120 °C prior to the nitrogen adsorption measurements. The adsorption isotherm was used to determine the pore size distribution using the Barret-Joyner-Halender (BJH) method, assuming a cylindrical pore modal. Powder X-ray diffraction (XRD) pattern was obtained on an X-ray diffractometer (Rigaku, Japan) using Cu Kα ray (λ = 1.54056 Å) as irradiation source with the scan rate of 0.05° 2θ s^{-1}. The accelerating voltage and applied current were 40 kV and 80 mA, respectively. Transmission electron microscopy (TEM) images and high-resolution transmission electron microscopy (HRTEM) images were taken on a JEM-2100 F electron microscope (JEOL, Japan) at an accelerating voltage of 200 kV.

2.4. Measurement of the photocatalytic activity

The photocatalytic activities of the obtained PE systems were evaluated in the photocatalytic degradation of the dyes in the water phase at ambient temperature. The experiments were performed as follows: First, an emulsion prepared according to Table 1 was directly transferred from the vial to a dish with a diameter of approximately 7.5 cm, and the dish was put in a circulating cooling water system to keep the temperature relatively constant. A 350 W Xe lamp positioned 50 cm directly above the dish was used as a light source to trigger the photocatalytic degradation reaction. Before irradiation, the system was left undisturbed in the dark for more than 4 h to reach the adsorption-desorption equilibrium between the dye and photocatalyst. At certain intervals of irradiation, 3 mL of the dye solution in the water phase was sampled to analyze the change in the concentration of the dye by a UV-2600 UV/Vis spectrophotometer (Shimadzu, Japan) and then poured back into the system. The degradation rates of the systems based on X_3B, MO, CR, and OG were determined from the changes in the intensity of the absorption peaks at 529, 464, 498, and 478 nm, respectively.

For comparison, traditional photocatalytic degradation processes were also carried out over a TiO_2 powder suspension and a TiO_2 film under the same experimental conditions in the absence of the oil phase. The mass of TiO_2 powder and the volume and concentration of the aqueous dye solution were decided according to Table 1. To prepare a TiO_2 film in the reactor, TiO_2 powder was first ultrasonically dispersed in 20 mL of DI water to form a homogeneous slurry and then transferred into the dish reactor and dried in an oven at 60 °C for approximately 3 h. After the water fully evaporated, the TiO_2 powder tightly and uniformly coated the dish, forming a film.

It should be noted that the density of DCM is greater than that of water, so the obtained o/w PE microcapsules sank below the water phase. Hence, both in an emulsion system and a traditional system, light would first transmit through the aqueous dye solution and then reach the catalyst surface, making the two types of systems comparable.

To identify the degradation products in water, the samples were analyzed by liquid chromatography-mass spectrometry (LC/MS). A Terra C-18 capillary column (2.1 μm × 150 mm length) was used to separate the product intermediates. The mobile phase was a mixture of acetonitrile and water that was filtered through a 0.22 μm Millipore syringe filter and had a volume ratio gradient. The flow rate of elute was 0.2 mL min^{-1}. MS analysis was performed in positive ion mode on a mass spectrometer equipped with an ESI ion source. The ESI probe tip and capillary potential were set to 2.5 kV and 25 V, respectively. The mass range was 50–1000 m/z.

3. Results and discussion

3.1. Pickering emulsion formation

It was very interesting and exciting to find that by adding a small amount of organic solvent (DCM) to a conventional photocatalytic reaction system (TiO_2 powder dispersed in an aqueous dye solution) before photoirradiation, an o/w PE was successfully generated by a simple manual shaking method. However, stable emulsions could not be obtained by shaking the TiO_2/DCM/water mixture without the dye molecules nor the mixture of DCM and aqueous dye solution without TiO_2 powder, implying that the dye molecules and TiO_2 powder played key roles in the one-step PE construction. Under the optimized emulsification conditions (Table 1), the obtained mixture formed two phases - a top clear dye solution and a bottom emulsion phase (insets of Fig. 1a–d). Optical microscopy images of the emulsion phase revealed the presence of discrete spherical microcapsules with diameters ranging from 15 to 150 μm (Fig. 1a–d, Fig. S2). The microcapsules remained stable against coalescence for more than one month under static, hermetic and dark conditions (Fig. S3).

Furthermore, the type of emulsion was identified by fluorescence microscopy. The calcein-tagged water phase (green fluorescence) was positioned around the microdroplets (Fig. 1e), while the Nile red-tagged oil phase (red fluorescence) was encapsulated within the microdroplets (Fig. 1f and g), indicating the formation of an o/w emulsion. Moreover, in the PE constructed via FITC-tagged TiO_2 powder, the particles were strictly located on the oil/water interface, and no fluorescence signals were observed inside or outside the microdroplets (Fig. 1h). This result further verified that the bare TiO_2 powder acted as an emulsifier to stabilize the o/w PE in the presence of specific dye molecules in the aqueous phase.

3.2. Interaction between dye and TiO_2

To understand why the commercial TiO_2 powder here could stabilize oil droplets in the aqueous dye solution without surface pretreatment, systematic characterizations were carefully conducted. Significantly, dye molecules in the system were thought to act as an indispensable cofactor because their hydrophobic aromatic framework and hydrophilic terminating groups render them to be an analogous surfactant. To confirm this, TiO_2 powder was dispersed in an aqueous X_3B solution in a vial and vibrated overnight. Then, the mixture was centrifuged at 10,000 rpm for 5 min, and the sediment was washed with DI water once by centrifugation. The obtained sample was dried at 60 °C overnight and defined as X_3B/TiO_2 for the surface characterization. Other samples, including MO/TiO_2, CR/TiO_2, and OG/TiO_2, were

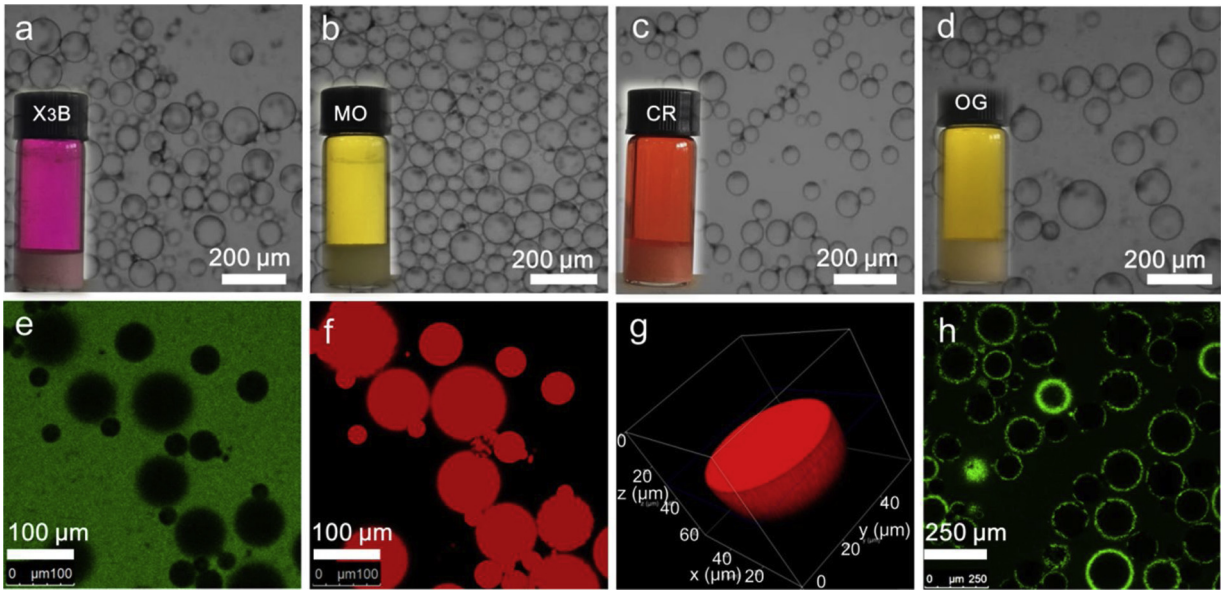

Fig. 1. Optical microscopy images and photographs (insets) of the PEs formed from (a) X_3B, (b) MO, (c) CR, and (d) OG based dispersions. (e–f) Fluorescence microscopy images of the X_3B/TiO_2-based PEs with added (e) calcein and (f) Nile red. (g) Three-dimensional image of the X_3B/TiO_2-based PE with added Nile red. (h) Fluorescence microscopy image of the FITC-labeled TiO_2 particles in the X_3B/TiO_2-based PE (For interpretation of the references to colour in this figure legend, the reader is referred to the web version of this article).

obtained via the same method. The concentration of the aqueous dye solution was displayed in Table 1.

The X_3B/TiO_2 powder exhibited a pink color and possessed the ability to stabilize DCM droplets in pure water without dye molecules (Fig. S4a). Its water contact angle (40°) exhibited an obvious increase than that of the bare TiO_2 (8.5°) (Fig. 2a and b). On the other hand, physical disassembly of the premade TiO_2/oil/X_3B PE by centrifugation resulted in the same pink TiO_2 powder that preferentially located at the interface between the water and oil phases, but not located at the bottom of the centrifuge tube (Fig. S4b,c). These results indicated that the X_3B molecules adhered to the particle surface and greatly changed the surface wettability of TiO_2.

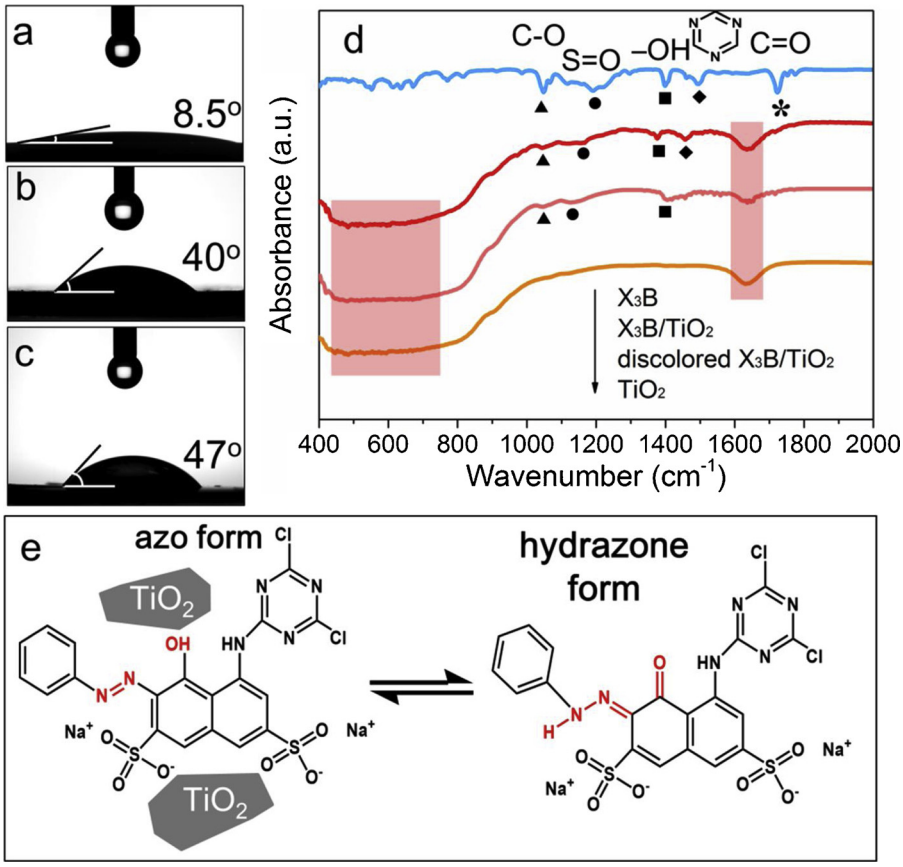

Fig. 2. Water contact angle of (a) the commercial TiO_2 powder (TiO_2), (b) the X_3B treated TiO_2 (X_3B/TiO_2) and (c) the recycled powder after the photocatalytic discoloring process (discolored X_3B/TiO_2). (d) Comparison of the FTIR spectra of the X_3B, X_3B/TiO_2, discolored X_3B/TiO_2, and TiO_2 samples. (e) Diagram of the interactions between TiO_2 and X_3B and the isomer structures of the azo and hydrazone forms of X_3B.

FTIR spectroscopy was employed to investigate the specific interactions between the TiO_2 particles and the dye molecules (Fig. 2d). In the FTIR spectrum of pure X_3B, several characteristic peaks could be distinguished in the region of 400–2000 cm^{-1}, as displayed in Table S1. [24,25] The coexistence of −OH and C═O bonds was not unexpected because a tautomeric intermolecular hydrogen bonding interaction occurs between the oxygen of the naphthyl group and the hydrogen of the azo bond [26,27]. Consequently, two isomers of the X_3B dye containing an azo form and a hydrazone form probably coexisted in the system (Fig. 2e).

By contrast, in the FTIR spectrum of the X_3B/TiO_2 sample, beside the fingerprint peaks of TiO_2 and the peak for its surface −OH groups (red dash areas in Fig. 2d), all the characteristic peaks of X_3B were presented, excepting the C═O vibration peak. It has been reported that the dye molecules like X_3B could adsorb on the surface of TiO_2 particles via the oxygen atoms of sulfonate ($–SO_3^-$) and hydroxyl (−OH) groups (Fig. 2e, left). [25,28] Therefore, the isomerization of the X_3B molecule did not occur to come into hydrazone form when its −OH group was used to link with TiO_2 particles, which explains the absence of the C═O peak in its FTIR spectrum. Notably, all the peaks related to X_3B in the spectrum of X_3B/TiO_2 were shifted more or less towards the lower wavenumbers than those in X_3B (Fig. 2d, Table S1), implying that the vibration modes of the functional groups were strongly disturbed by the interaction with TiO_2 particles. Similarly, the dyes MO, CR and OG with $–SO_3^-$ (and −OH) groups in their molecular structures (Fig. S5) could also tightly adhere to the TiO_2 surface through Ti-O linkages, [25] which could be reflected from different perspectives by a less negative zeta potential, a reduced conductivity, an enhanced UV/vis diffuse reflectance absorption intensity of the TiO_2 after the dye adsorption, and decreased specific surface area (Fig. S6, Table S2). Such close association between the dye molecules and TiO_2 surface is of great significance for PE formation and photocatalytic reactions. Other dyes not containing $–SO_3^-$ groups, such as Eosin Y, rhodamine B, and methylene blue, were not able to play similar role in PE construction (not shown here). On the other hand, although some dyes such as Irgalite Red D, Cromophtal K, Paliotol Yellow K and Cromophtal Violet D could act as excellent Pickering stabilizers by themselves, which was found by Binks et al. recently, [29] they are not able to adhere on the surface of TiO_2 photocatalyst and possess a very low solubility in both water and oil due to their characteristic chemical structures. Therefore, these dyes are also unserviceable in our designed PE photocatalysis systems.

3.3. Photocatalytic performance

Although the surface properties of TiO_2 were greatly affected by dye treatment, the inherent properties of TiO_2 such as crystal structure and morphology were not influenced apparently (Fig. S7), which would guarantee its activity in photocatalytic reactions. Consequently, the photocatalytic performance of the formed PEs was evaluated in the dye degradation and compared with that of the traditional nonemulsified photocatalytic systems (mainly powder-solution and film-solution systems) under the same conditions. The dye molecules used to assist the PE construction were also used as model water pollutants in this study. Considering the self-degradation of the dyes and the possible influence of the oil phase on the dye degradation rate, the degradation of a pure aqueous dye solution and a mixture of aqueous dye solution and DCM was also carried out under the same experimental conditions. For simplicity, the studied systems of a pure dye solution (W), a dye solution-DCM mixture (W + O), TiO_2 film in dye solution (W + S_{film}), TiO_2 powder in dye solution (W + S_{powder}), and PE were identified as systems i, ii, iii, iv, and v, respectively, as shown in Table 2. Note that the mass of TiO_2 powder and the volumes of the aqueous dye solution and DCM used in the degradation experiment were determined according to Table 1, and for the same dye in different systems, the amount of TiO_2 powder, aqueous dye solution and DCM were kept constant.

Fig. 3a depicts a comparison of the X_3B concentration changes during the photocatalytic process in each of the different systems. Under light irradiation (350 W Xe lamp), the aqueous X_3B solution (i) exhibited slight self-degradation. When DCM oil was added (ii), the self-degradation rate was enhanced to a certain degree, suggesting that the presence of DCM boosted X_3B degradation. Gratifyingly, the decomposition of X_3B in the PE system (v) was almost complete within only 30 min of irradiation, following the pseudo-first-order reaction (Fig. S8g). [30] The corresponding apparent rate constants (k) was much higher than that of the film-solution (iii) and powder-solution (iv) systems (Fig. 3b, Table 2). The relevant color changes of the dye solutions in systems iii and v during irradiation are displayed in Fig. S9. It demonstrated that the PE-based systems exhibited superior photocatalytic performance in dye degradation comparing to the traditional photocatalytic systems, which is in line with our expectations. In addition to X_3B, a similar phenomenon occurred in the photocatalytic degradation of the other dyes, MO, CR, and OG (Fig. 3b, Fig. S8).

Table 2
Comparison of the apparent rate constants (k) of photocatalytic dye degradation in different systems.

No.	System[a]	k (10^{-3} min^{-1})			
		X_3B	MO	CR	OG
i	W	1.9	1.3	0.2	0.5
ii	W + O	9.3	6.4	9.7	2.4
iii	W + S_{film}	15.5	12.8	17.5	7.4
iv	W + S_{powder}	76.7	21.1	26.8	33.6
v	PE	165.0	71.0	224.9	44.2

[a] W, O, S_{film} and S_{powder} refer to the pure dye solution, DCM, the TiO_2 film, and TiO_2 powder, respectively.

The other advantage of the PE system is that the photocatalysts could be easily recovered from the reaction system for reuse. After decolorization of the dye for 30 min, the upper decolorized solution was replaced with isometric fresh dye solution, and another cycle of photodegradation was performed for 30 min. This reaction cycle was repeated 4 times, during which the degradation rate remained nearly stable with only a slight decline (Fig. 3c). In addition, the microcapsules were still not broken after 4 cycles for a total of 2 h of irradiation (Fig. 3d). Note that some degree of coalescence and rearrangement of the PE microcapsules occurred in the first 30 min-irradiation period, resulting in obviously increased capsule size by approximately 430% (Fig. S10). It is because the amphipathy of the TiO_2 particles changed dynamically since the surface-adsorbed dye molecules were gradually degraded and new ones from the solution simultaneously replaced them. Once this dynamic process reached equilibrium, the microcapsule size remained relatively stable, with only approximately 30%, 3% and 15% increases during the second, third and fourth degradation cycles, respectively (Fig. S10). The results demonstrated that the PE system constructed from a dye/TiO_2 mixture could withstand long-term irradiation without severe demulsification, which satisfactorily meets the requirement of practice photocatalysis applications. It is worthy to note that, with the microcapsules becoming larger after each degradation cycle, the total effective contact areas between TiO_2 and dye molecules were kindly decreased, which explained one of the reasons of the slightly-decreased photoactivity after degradation cycles.

Moreover, it is surprised to find that the PE microcapsules remained integrity under continuous light irradiation for as long as 6 h. Similarly, the size of the microdroplets increased significantly within 1 h and then plateaued for 5 h until shrinking after 7 h and disassembling after 8 h (Fig. S11). As demonstrated earlier, the dye molecules played a key role in the construction of the PE in this study. However, after complete decolorization of the dye within 30 min, the emulsions still remained unbroken for another 5.5 h, which might be attributed to the intermediate products of degradation.

Indeed, although the UV–vis absorption spectra of the aqueous

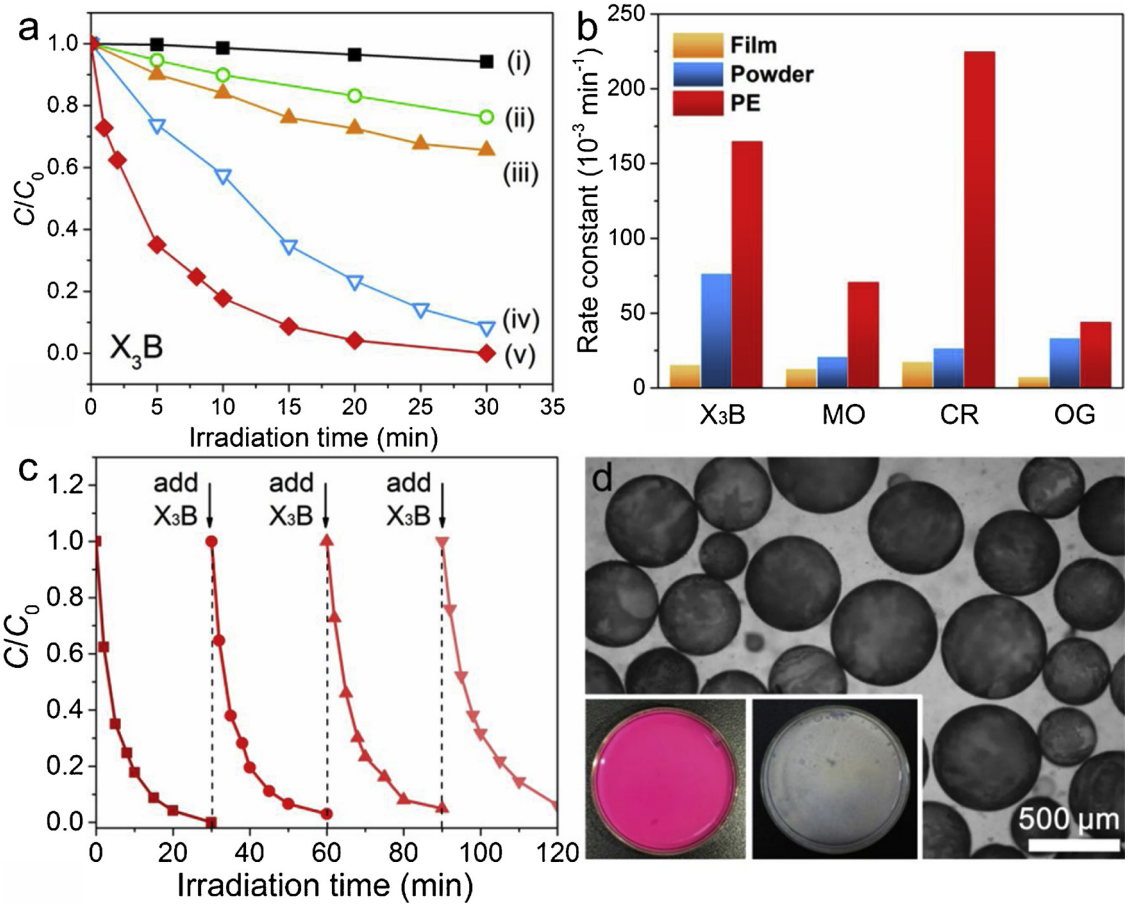

Fig. 3. (a) Comparison of the X_3B concentration changes during photocatalysis by the systems i–v. (b) Comparison of the apparent rate constants for photocatalytic dye degradation by the systems iii–v. (c) Four photocatalytic cycles of X_3B degradation in the PE system. (d) Optical microscopy image of the emulsion after completion of the fourth photocatalytic cycle; the inset is pictures of the reaction system before and after irradiation for 2 h.

phase showed a gradual decline in the three peaks at 205, 311, and 530 nm (corresponding to the benzene ring, naphthalene ring, and azo linkages, respectively) over the course of 30 min irradiation (Fig. 4e), [24] suggesting that the initial X_3B molecules in the aqueous solution were almost degraded, a small amount of X_3B (A) and the intermediate degradation products 2-(phenyldiazenyl)naphthalen-1-ol (B), 2,8-diaminonaphthalen-1-ol (C), and 4,6-dichloro-1,3,5-triazin-2-amine (D) were still detected in the liquid chromatography-mass spectrometry (LC/MS) spectra of the water phase after 30 min (Fig. 4a–c, Table 3); these products correspond to the breakage of four possible bonds in X_3B (Fig. 4d). The existence of those fragments in the water phase might contribute to keep the PE intact, because they also have the typical amphiphilic characteristics to modulate the TiO_2 surface wettability. This suggestion was evidenced from a side by the successful PE formation, with the phenylenediamine modified TiO_2 as the stabilizer, and pure water and DCM as the water and oil phase, respectively (Fig. S12), wherein the phenylenediamine with a benzene ring and two amino groups has a similar characteristic with the product C in Table 3. Further evidences come from the test results of water contact angle (Fig. 2c), FTIR spectrum (Fig. 2d), and specific surface area (S_{BET}) (Fig. S6c) of the powder recycled from the PE system after the photocatalytic decolorization process, which was named as discolored X_3B/TiO_2. The water contact angle of the discolored X_3B/TiO_2 (47°) was even larger than that of the X_3B/TiO_2 (40°), and the FTIR result showed that the C—O bond, —SO_3^- group, and —OH group still existed in the discolored X_3B/TiO_2 sample. The S_{BET} of the commercial TiO_2 (155.1 $m^2 g^{-1}$) became smaller after the X_3B decoration (140.0 $m^2 g^{-1}$ for the X_3B/TiO_2), and even smaller after the dye decolorization (108.5 $m^2 g^{-1}$ for the discolored X_3B/TiO_2), owing to the partial filling or blocking of the meso/macroporous structures in TiO_2 after the decoration by X_3B molecules and their intermediate product fragments, respectively. These results pointed to the same conclusion that the intermediate products of X_3B degradation tightly attached on the surface of TiO_2 and maintained its surface wettability.

However, with the mineralization process going more thorough over time, the amount of the amphipathic intermediate products from dyes was too small to keep the TiO_2 particles stay at the oil/water interface. Thereafter, the PE was ultimately disassembled after 8 h irradiation. Further studies on this interesting system are underway with the goal of clarifying the relationships between the mineralization degree of the dye molecules, the surface properties of the TiO_2 particles, and characters of the PE microcapsules in detail.

On the other hand, the UV–vis absorption spectra of the oil phase within the PEs during the 30 min irradiation revealed an increase in the intensity of the peaks at 228 and 268 nm, suggesting the increased concentration of aromatic compounds in the oil phase (Fig. 4f). These results implied that some oleophilic by-products were extracted into the oil phase of the PE during the course of degradation, which would spatially separate the reactants from the products and thereby accelerate the forward reaction. Similar phenomena have been reported in previous literatures. [31,32] The slight increase in the size of the microcapsules from the second to the fourth cycle of the reaction (Fig. S10) was also possibly due to the enrichment of oleophilic products to the oil phase. Such changed compositions of PE might be another reason of the slightly-decreased photoactivity after four recycles as shown in Fig. 3c. However, the anoxic environment in the oil droplets would be helpful to protect these by-products from further mineralization, which is possibly beneficial for the reclamation and reuse of

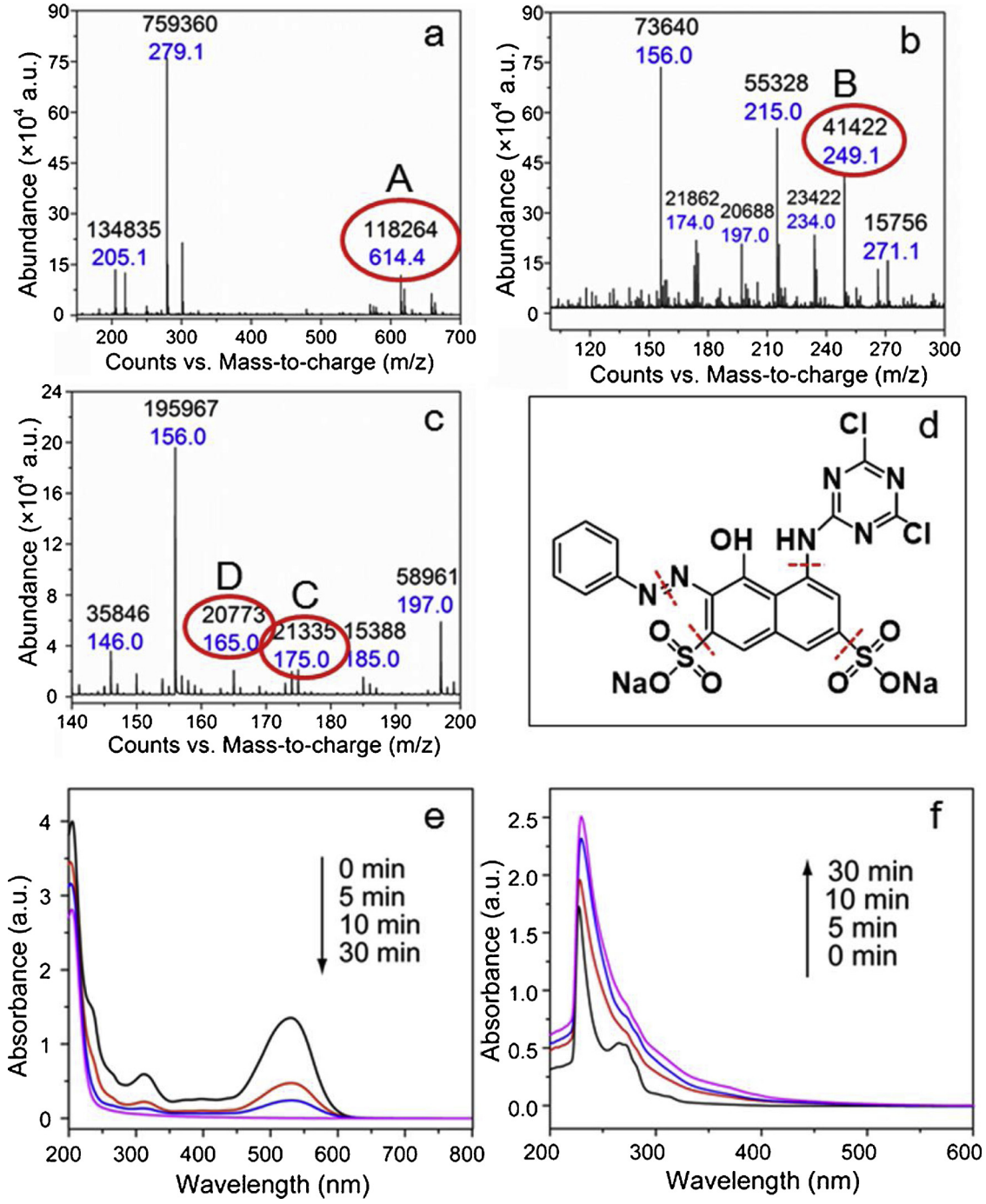

Fig. 4. (a–c) LC/MS spectra of X_3B degradation products in the water phase. (d) Possible bond-breaking positions in the X_3B molecule. UV–vis spectra of (e) the water and (f) oil phases during the X_3B degradation over 30 min in the PE system.

some specific intermediate products of dyes to be important raw materials in chemical industries.

Based on the results above, a possible photocatalytic model was proposed for the Pickering emulsion system. As illustrated in Scheme 1, with the help of the target pollutant (dye molecules) in water, the TiO_2 semiconductor nanoparticles served as an emulsifier for the PE without any introduction of foreign modifiers. Under light irradiation, the dye molecules adsorbed on the surface of the TiO_2 particles were the first to react with the photogenerated active species from the photocatalyst (TiO_2) and gradually degraded into fragments. Among them, some hydrophilic intermediate products stayed in the water phase and absorbed on TiO_2 surface to maintain its suitable wettability. Therefore, the PE could withstand long-time irradiation and exhibited good recyclability. Besides, some oleophilic intermediate products were extracted into the oil phase (DCM) and were protected from further mineralization due to the anoxic environment. Such separation of reactants and products in different liquid phases would accelerate the forward reaction to a large extent, and induced the much enhanced photoactivity of PE system than those in the traditional systems.

4. Conclusions

In summary, we developed a novel and handy strategy to build Pickering emulsions directly via commercial TiO_2 particles without prior surface modification processes by adding foreign modifiers. In the water phase, the dye molecules with characteristic sulfonate groups

Table 3
The chemical structure of X_3B and its degradation products.

No.	Chemical structure	Name (Chemical formula)	M
A	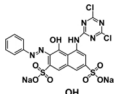	X_3B ($C_{19}H_{10}O_7N_6Cl_2S_2Na_2$)	613.9
B	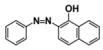	2-(phenyldiazenyl)naphthalen-1-ol ($C_{16}H_{12}N_2O$)	248.1
C		2,8-diaminonaphthalen-1-ol ($C_{10}H_{10}N_2O$)	174.1
D		4,6-dichloro-1,3,5-triazin-2-amine ($C_3N_4H_2Cl_2$)	164.0

tightly adhered on the surface of TiO_2 powder and changed its wettability via the exposed hydrophobic groups, thus empowering TiO_2 to be an emulsifier. The prepared Pickering emulsions not only exhibited significantly enhanced photocatalytic efficiency over the traditional non-emulsified systems, but also showed excellent recyclability for reuse under long-time irradiation. This new strategy for Pickering emulsion construction is technically simple and potentially applicable to many other semiconductors and suitable targeted reactants in water or oil phases. Consequently, it is believed that this study creates a paradigm for future studies of novel Pickering emulsion-based photocatalytic systems in various applications such as environmental decontamination, water splitting, artificial photosynthesis, biocatalysis, and so on.

Acknowledgements

National Natural Science Foundation of China (21571192, 21503281), Fundamental Research Funds for the Central Universities, South-Central University for Nationalities (CZT19008), and Natural Science Foundation of South–Central University for Nationalities (YZZ14001, XTZ15016).

Appendix A. Supplementary data

Supplementary material related to this article can be found, in the online version, at doi:https://doi.org/10.1016/j.apcatb.2019.02.057.

References

[1] S.U. Pickering, Emulsions, J. Chem. Soc. Trans. 91 (1907) 2001–2021.
[2] P.F. Marina, J. Xu, X. Wu, H.L. Xu, Thinking outside the box: placing hydrophilic particles in oil phase for formation and stabilization of Pickering emulsions, Chem. Sci. 9 (2018) 4821–4829.
[3] B. Jiao, A.M. Shi, Q. Wang, B.P. Binks, High internal phase Pickering emulsions stabilized solely by peanut protein microgel particles with multiple potential applications, Angew. Chem. Int. Edit. 57 (2018) 9274–9278.
[4] H.Q. Yang, T. Zhou, W.J. Zhang, A strategy for separating and recycling solid catalysts based on the pH-triggered Pickering-emulsion inversion, Angew. Chem. Int. Edit. 52 (2013) 7455–7459.
[5] Y. Fadil, F. Jasinski, T. Wing Guok, S.C. Thickett, H. Minami, P.B. Zetterlund, Pickering miniemulsion polymerization using graphene oxide: effect of addition of a conventional surfactant, Polym. Chem. 9 (2018) 3368–3378.
[6] Q. Cao, Q.L. Cui, Y. Yang, J.S. Xu, C.H. Han, L.D. Li, Graphitic carbon nitride as a distinct solid stabilizer for emulsion polymerization, Chem. Eur. J. 24 (2018) 2286–2291.
[7] C.H. Han, Q.L. Cui, P. Meng, E.R. Waclawik, H.Q. Yang, J.S. Xu, Direct observation of carbon nitride-stabilized Pickering emulsions, Langmuir 34 (2018) 10135–10143.
[8] P.R. Wei, Q.M. Luo, K.J. Edgehouse, C.M. Hemmingsen, B.J. Rodier, E.B. Pentzer, 2D particles at fluid–fluid interfaces: assembly and templating of hybrid structures for advanced applications, ACS Appl. Mater. Interfaces 10 (2018) 21765–21781.
[9] Y. Ding, H. Xu, H.H. Wu, M.Y. He, P. Wu, An amphiphilic composite material of titanosilicate@mesosilica/carbon as a Pickering catalyst, Chem. Commun. 54 (2018) 7932–7935.
[10] T. Burdyny, J. Riordon, C.T. Dinh, E.H. Sargent, D. Sinton, Self-assembled nanoparticle-stabilized photocatalytic reactors, Nanoscale 8 (2016) 2107–2115.
[11] C.H. Han, P. Meng, E.R. Waclawik, C. Zhang, X.H. Li, H.Q. Yang, M. Antonietti, J.S. Xu, Palladium/graphitic carbon nitride (g-C_3N_4) stabilized emulsion microreactor as a store for hydrogen from ammonia borane for use in alkene hydrogenation, Angew. Chem. Int. Ed. 57 (2018) 14857–14861.
[12] J.S. Xu, M. Antonietti, The performance of nanoparticulate graphitic carbon nitride as an amphiphile, J. Am. Chem. Soc. 139 (2017) 6026–6029.
[13] Y.Q. He, F. Wu, X.Y. Sun, R.Q. Li, Y.Q. Guo, C.B. Li, L. Zhang, F.B. Xing, W. Wang, J.P. Gao, Factors that affect Pickering emulsions stabilized by graphene oxide, ACS Appl. Mater. Interfaces 5 (2013) 4843–4855.
[14] C. Mccullagh, N. Skillen, M. Adams, P.K.J. Robertson, Photocatalytic reactors for environmental remediation: a review, J. Chem. Technol. Biotechnol. 86 (2011) 1002–1017.
[15] Q. Li, X. Li, S. Wageh, A.A. Al-Ghamdi, J.G. Yu, CdS/graphene nanocomposite photocatalysts, Adv. Energy Mater. 5 (2015) 1500010.
[16] M.F. Nsib, A. Maayoufi, N. Moussa, N. Tarhouni, A. Massouri, A. Houas, Y. Chevalier, TiO2 modified by salicylic acid as a photocatalyst for the degradation of monochlorobenzene via Pickering emulsion way, J. Photochem. Photobiol. A 251 (2013) 10–17.
[17] T. Nakato, H. Ueda, S. Hashimoto, R. Terao, M. Kameyama, E. Mouri, Pickering emulsions prepared by layered niobate $K4Nb_6O_{17}$ intercalated with organic cations and photocatalytic dye decomposition in the emulsions, ACS Appl. Mater. Interfaces 4 (2012) 4338–4347.
[18] W. Wu, S. Gao, W.X. Tu, J.F. Chen, P.Y. Zhang, Intensified photocatalytic degradation of nitrobenzene by Pickering emulsion of ZnO nanoparticles, Particuology 8 (2010) 453–457.
[19] W.Y. Zhai, G.P. Li, P. Yu, L.F. Yang, L.Q. Mao, Silver phosphate/carbon nanotube-stabilized Pickering emulsion for highly efficient photocatalysis, J. Phys. Chem. C 117 (2013) 15183–15191.
[20] S.Y. Guo, Y.N. Jiang, F. Wu, P. Yu, H.B. Liu, Y.L. Li, L.Q. Mao, Graphdiyne-promoted highly efficient photocatalytic activity of graphdiyne/silver phosphate Pickering emulsion under visible-light irradiation, ACS Appl. Mater. Interfaces (2018), https://doi.org/10.1021/acsami.8b04463.
[21] B.P. Binks, J.H. Clint, Solid wettability from surface energy components: relevance to Pickering emulsions, Langmuir 18 (2002) 1270–1273.
[22] S. Santra, B. Liesenfeld, C. Bertolino, D. Dutta, Z. Cao, W. Tan, B.M. Moudgil, R.A. Mericle, Fluorescence lifetime measurements to determine the core–shell nanostructure of FITC-doped silica nanoparticles: an optical approach to evaluate nanoparticle photostability, J. Luminescence 117 (2006) 75–82.
[23] Y.L. Wang, J. Wang, X.Y. Deng, J. Wang, H.F. Wang, M.H. Wu, Z. Jiao, Y.F. Liu, Direct imaging of titania nanotubes located in mouse neural stem cell nuclei, Nano Res. 2 (2010) 543–552.
[24] M. Stylidi, Pathways of solar light-induced photocatalytic degradation of azo dyes in aqueous TiO_2 suspensions, Appl. Catal. B: Environ. 40 (2003) 271–286.
[25] C. Bauer, P. Jacques, A. Kalt, Investigation of the interaction between a sulfonated azo dye (AO7) and a TiO_2 surface, Chem. Phys. Lett. 307 (1999) 397–406.
[26] P. Ball, C.H. Nicholls, Azo-hydrazone tautomerism of hydroxyazo-compounds-a review, Dyes Pigments 3 (1982) 5–26.
[27] M. Stylidi, Visible light-induced photocatalytic degradation of acid Orange 7 in aqueous TiO_2 suspensions, Appl. Catal. B: Environ. 47 (2004) 189–201.
[28] F.L. Zhang, J.C. Zhao, T. Shen, H. Hidaka, E. Pelizzetti, N. Serpone, TiO_2-assisted photodegradation of dye pollutants II. Adsorption and degradation kinetics of eosin in TiO_2 dispersions under visible light irradiation, Appl. Catal. B: Environ. 15 (1998) 147–156.
[29] B.P. Binks, S.O. Olusanya, Pickering emulsions stabilized by coloured organic pigment particles, Chem. Sci. 8 (2017) 708–723.
[30] J.G. Yu, Q. Li, S.W. Liu, M. Jaroniec, Ionic-liquid-assisted synthesis of uniform fluorinated B/C-codoped TiO_2 nanocrystals and their enhanced visible-light photocatalytic activity, Chem. Eur. J. 19 (2013) 2433–2441.
[31] C. Yu, L.M. Fan, J. Yang, Y.Y. Shan, J.S. Qiu, Phase-reversal emulsion catalysis with CNT-TiO_2 nanohybrids for the selective oxidation of benzyl alcohol, Chem. Eur. J. 19 (2013) 16192–16195.
[32] S. Crossley, J. Faria, M. Shen, D.E. Resasco, Solid nanoparticles that catalyze biofuel upgrade reactions at the water/oil interface, Science 327 (2010) 68–72.